Efficient Electron Injection from Twisted Intramolecular Charge Transfer (TICT) State of 7-Diethyl amino coumarin 3-carboxylic Acid (D-1421) Dye to TiO_2 Nanoparticle

G. Ramakrishna and Hirendra N. Ghosh*

Radiation Chemistry & Chemical Dynamics Division, Bhabha Atomic Research Center, Trombay, Mumbai 400 085, India

Received: October 15, 2001; In Final Form: December 17, 2001

Electron injection and back-electron-transfer dynamics of 7-diethyl amino coumarin 3-carboxylic acid (D-1421) and coumarin 343 (C-343) dyes adsorbed on TiO_2 nanoparticles have been studied by picosecond transient absorption and time-resolved fluorescence spectroscopy. Electron injection has been observed by direct detection of electron in the conduction band of nanoparticle and cation radical of the dyes as detected by picosecond transient absorption spectroscopy. Electron injection efficiency has been found to be much higher for D-1421-sensitized TiO_2 nanoparticle compared to C-343-sensitized TiO_2 nanoparticle system. Steady state and time-resolved fluorescence measurements show that in high polar solvent, the excited state of D-1421 dye molecule predominantly exits as twisted intramolecular charge transfer (TICT) state, whereas excited C-343 exists as intramolecular charge transfer (ICT) state. On excitation with a laser pulse, D-1421 dye molecule in a highly polar solvent (water) goes to the ICT state and then relaxes very fast to the TICT state. Electron injection for D-1421 dye can take place both from ICT state and TICT state. As TICT is a highly charge-separated state, it can inject electrons very efficiently to the TiO_2 nanoparticle. Quantum yield for electron injection for D-1421 dye has been found to be 0.90 compared to 0.60 for C-343.

1. Introduction

Dye sensitization of wide band semiconductor electrodes has gained sufficient attention in recent years, largely because of the demonstration of the dye-sensitized solar cells with conversion efficiency as high as 10%.[1,2] The mechanism of solar cell devices is based upon the injection of an electron from a photoexcited state of the sensitized dye into the conduction band of the semiconductor. The efficiency of the dye-sensitized solar cells depends critically on the rates of the forward (dye to semiconductor) and back (semiconductor to dye) electron-transfer reactions. For an efficient solar energy conversion it is necessary to establish the conditions of both fast electron injection and slow recombination. High yield of long-lived charge separation is expected for the useful conversion of sunlight into electric charge. However, detailed mechanisms, the nature, and the rate of electron injection into the semiconductor, and factors determining the rate of back-electron-transfer, are not well understood. Reports are available on back ET rates for different adsorbate dyes on nanoparticles ranging from picoseconds,[3−12,23−30] nanoseconds[3−5,13−18] up to microseconds,[5,19−22] and even milliseconds.[19−21] On the contrary, not many experimental reports are available on injection kinetics, except for some reports by Durrant et al.,[31] where they have shown that injection kinetics are insensitive to variation of experimental conditions such as electrolyte concentration and application of electrical bias.[31] Effect of bridge length of the binding ligand of Re-polypyridyl complexes on electron injection kinetics in TiO_2 nanocrystalline thin film was studied by Asbury et al.[32] They have observed that the introduction of the $-CH_2$ group in the bridging length can retard the electron injection process. Evidence of hot excited-state electron injection from sensitizer to TiO_2 nanocrystalline thin film was also studied by Asbury et al.[33] They have reported that electron injection occurred during or prior to electronic and vibrational relaxation of the sensitizer molecules in the excited state.

Electron injection process in dye-sensitized nanoparticle can takes place followed by charge separation within the excited state of the dye molecule. To understand the mechanism of electron injection, it is very important to know the property of the dye molecule in the excited state. The structural effect of different Ru-dye molecules on charge separation (CS) process of photoinduced dye-TiO_2 systems has been compared by Gratzel et al.[34] They have observed that the charge separation efficiency depends on the localization of the electron in the excited state of the chromophore. The best CS yield was obtained for the system in which the localization occurs on the ligand bound to the semiconductor surface. The behaviors of the excited-state dye molecules can be monitored by transient absorption and fluorescence spectroscopy. Aromatic compounds possessing two chromophores and exhibiting dual fluorescence are of great interest[35−38] because the additional fluorescence is frequently associated with the formation of a highly polar excited electronic structure. Such polar forms usually originate in the transfer of an electron from a chromophore to another within the molecular structure, a process that is involved in some highly significant, naturally occurring mechanisms such as vision and photosynthesis.[39] Every charge separation process in a chromophore is favored by a polar environment, solvent polarity is believed to facilitate the formation of the more polar forms through increased viability of a twisted intramolecular charge transfer (TICT) mechanism. In any case, it is obvious that if the solvent polarity induces a change in the excited electronic state leading to high polar form through charge separation within the molecule, then that can induce electron injection in to the conduction band of the TiO_2 nanoparticle.

In the present investigation we have studied electron injection and back-electron-transfer dynamics of 7-diethyl amino coumarin-3-carboxylic acid (D-1421) and coumarin 343 (C-343) dyes (Figure 1) adsorbed on TiO_2 nanoparticles using picosecond transient absorption and time-resolved fluorescence spectro-

* Corresponding author. E-mail: hnghosh@magnum.barc.ernet.in. Fax: 00-91-22-5505151.

10.1021/jp013803x CCC: $22.00
Published on Web 02/19/2002

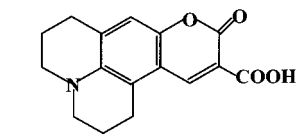

C343

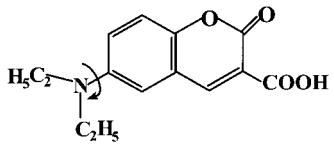

D 1421

Figure 1. Molecular structure of the coumarin dyes studied in the present work.

scopy. The electron injections to the TiO_2 nanoparticle by D-1421 and C-343[3] have been confirmed by picosecond transient absorption studies, where the cation of the dye molecule and conduction band electron in the nanoparticle have been detected in the visible region. To see the effect of molecular structure of the dye on electron injection, these two dyes are chosen. Both the dyes have the same anchoring groups, which bind to the TiO_2 nanoparticle with a similar structure, except that D-1421 has the diethyl amino group, and the nitrogen atom is in the ring for C-343 (Figure 1). Steady-state and time-resolved fluorescence measurements show that excited D-1421 molecule predominantly exists as twisted intramolecular charge transfer (TICT) state after photoexcitation, whereas excited C-343 exists as an intramolecular charge transfer (ICT) state. Time-resolved absorption studies show that electron injection efficiency is much higher (1.5 times) in the case of D-1421-sensitized TiO_2 nanoparticle compared to C-343-sensitized nanoparticle in a similar condition. The results have been explained in the following fashion. On excitation by a laser pulse, the C-343 molecule goes to the excited state and then the electron injection takes place from the excited state of the dye molecule to the nanoparticle. In the case of D-1421, on photoexcitation the molecule goes to the intramolecular charge transfer (ICT) state and then it relaxes very fast to the TICT state. Because the TICT state is in a higher charge separated state compared to the ICT state, charge separation takes place very efficiently within the molecule in TICT state. So, electron injection is very efficient from the TICT state compared to that from the ICT state. On the other hand, relaxation from TICT state to ground state is a forbidden transition, so TICT has a higher lifetime compared to that of the ICT state. As a result, electron injection is more efficient from the TICT state than from the ICT state. In the present investigation we have observed that the TICT state of the D-1421 molecule is nonemissive. But in the presence of low TiO_2 nanoparticle concentration, emission from the TICT state of the D-1421 dye molecule has been detected. Rate of back-electron-transfer reaction from the TiO_2 nanoparticle to the parent cation has been monitored from the decay of the transient absorption of the cation radicals.

2. Experimental Section

(a) Materials. Coumarin 343 (C-343) from Aldrich (97%) and 7-diethyl amino coumarin 3-carboxylic acid (D-1421) from Molecular Probes were used without further purification. Titanium (IV) tetra-isopropoxide $\{Ti[OCH(CH_3)_2]_4\}$ (Aldrich, 97%) and isopropyl alcohol (Aldich) were purified by distillation. Zirconium (IV) isopropoxide 2-propanol complex $Zr[OCH(CH_3)_2]_4$ $(CH_3)_2CHOH$ (Aldrich, 99.9%) was used without further purification. Nanopure water was used for making aqueous solutions.

(b) Sample Preparation. Nanometer-size TiO_2 was prepared by controlled hydrolysis of titanium (IV) tetraisopropoxide.[3,40,41] A solution of 5 mL of $Ti[OCH(CH_3)_2]_4$ (Aldrich, 97%) dissolved with 95 mL of isopropyl alcohol (Aldich) was added dropwise (1 mL/min) to 900 mL of Nanopure water (2 °C) at pH 1.5 (adjusted with HNO_3). The solution was continuously stirred for 10−12 h until a transparent colloid was formed. The colloidal solution was concentrated at 35−40 °C with a rotary evaporator and then dried with nitrogen stream to yield a white powder. ZrO_2 nanoparticle was also prepared by adopting the above procedure. In the present work all colloidal samples were prepared after dispersing the dry TiO_2 nanoparticles in water (15 g/L). A transparent clear solution of TiO_2 nanoparticle was formed. To prepare sensitized nanoparticles, coumarin dyes were added to TiO_2 colloid and sonicated for 1 min. For all the measurements the sample solutions were deoxygenated by continuously bubbling high purity nitrogen (99.95 IOLAR grade from Indian Oxygen Co. Ltd., India) through the solutions. The solutions were passed through a 1 cm × 1 cm quartz cell during all the measurements.

(c) Picosecond Visible Spectrometer. Picosecond laser flash photolysis experiments were carried out using a pump−probe spectrometer, described elsewhere.[42] Briefly, the second harmonic output (532 nm, 8 mJ, 35 ps) of an active-passive mode locked Nd:YAG laser (Continuum, USA, model 501-C-10) was used for the excitation of the samples. The transients produced in the irradiated samples were detected by their optical absorption. A white light continuum (∼400−950 nm) produced by focusing the residual fundamental (1064 nm) of the Nd:YAG laser onto a 10 cm length quartz cell containing 50:50 (v/v) H_2O-D_2O mixture was used as the monitoring light source. The probe light was passed through a variable optical delay line (1 m long) and then split into two parts using a 50:50 beam splitter. One part of the monitoring light was used as the reference beam and the other was used as the analyzing beam (passing through the irradiated sample). Both the reference and the analyzing beams were dispersed through a spectrograph and monitored using a dual diode array based optical multichannel analyzer, which is interfaced to a personal computer to process the data.

(d) Picosecond Time-Resolved Fluorimeter. Fluorescence lifetime measurements were carried out at the Tata Institute of Fundamental Research, Mumbai, using a time-resolved fluorescence measurement set up. The instrument works on the principle of time-correlated single photon counting (TCSPC) technique.[43] Briefly, the output of a picosecond (4 ps) titanium: saphire laser (Spectra Physics, Tsunami) at around 890 nm (average power ∼ 1 W, frequency ∼ 82 MHz) was passed through a pulse picker to reduce its frequency to about 800 kHz (with average power of about 15 mW). The 890 nm laser pulse was then used to generate second harmonic at 445 nm with an average power of about 1 mW. The second harmonic light was used to excite the sample. A small part of the reflected 445 nm light was used to generate the start pulse for the TCSPC instrument. The fluorescence signal gave the stop pulse for the TCSPC. Observed fluorescence decays were analyzed by a reconvolution procedure using a proper instrument response function, obtained by substituting the sample cell with a light scatterer. Decay curves were fitted either as a single exponential or multiexponential functions as

$$F(t) = \Sigma F_i(0) \exp(-t/\tau_i)$$

where τ_i is the emission lifetime and $F_i(0)$ is the preexponential factor of the ith component of the sample.

(e) Pulse Radiolysis. Transient absorption studies were carried out using pulse radiolysis technique described earlier.[44] Electron pulses of 7 MeV and 50 ns duration were used for irradiation. The transients produced were detected by kinetic spectrophotometer. The absorbed radiation dose was measured by thiocyanate dosimetry.[45] The typical dose was 10 Gy.

(f) Cyclic Voltametry. Voltametric experiments were performed with Auto Lab PGSTAT 20 (Manufactured by Eco-Chemie, The Netharlands) using Pt electrode (GC)/Pt/Ag/AgCl. The PG STAT was driven by Auto lab software. The temperature of the solution maintained at 25 ± 0.1 C°. The measurements were done in acetonitrile solution with TEAP (tetraethylammonium per chlorate) as supporting electrolyte and in N_2 atmosphere.

3. Results and Discussion

(a) Assignment of Steady-State Optical Absorption and Emission Spectra. To study the electron-transfer processes in D-1421-sensitized TiO_2 nanoparticle system, steady-state absorption and emission experiments have been carried out. It has been observed that, in the presence of TiO_2 nanoparticles, D-1421 dye molecules adsorb on the nanoparticle surface. Figure 2 shows the absorption spectrum of free D-1421 in water and D-1421-sensitized TiO_2 nanoparticles both at pH 2.5. The effect of increasing TiO_2 concentration on the absorption spectrum is also shown. Free D-1421 dye in water gives absorption peak at 435 nm at pH 2.5. The optical absorption spectra of these coumarin dyes are very sensitive to solution pH. Although we have observed in the pH range 1−4, the optical absorption spectra of these coumarin dyes do not change much. On addition of TiO_2 nanoparticle, the optical density at the absorption peak (435 nm) increases, goes broad and little red shifted. At higher concentration of TiO_2, the absorption spectrum shows a peak around 440 nm and it has absorption up to 600 nm. The pH of all the above experimental solutions is kept at 2.5. Benesi−Hilderband plot for the D-1421-TiO_2 nanoparticle system has been shown in Figure 2 inset. The equilibrium constant (K_{eq}) can be determined using Benesi−Hilderband equation.[46] For surface adsorbed dye molecules the equilibrium can be represented as

$$R{-}COO^- + = Ti{-}OH_2^+ \xrightarrow{K_{eq}} = Ti{-}OOC{-}R + H_2O$$

Since the particle concentration is proportional to the concentration of surface hydroxyl groups (≡Ti−OH_2^+), we can define the equilibrium constant as

$$K_{eq} = \frac{[Ti - OOCR]}{[R - COO^-][TiO_2]}$$

where [R−COO^-] is the concentration nonadsorbed dye, [TiO_2] the particle concentration, and [Ti−OOCR] is the concentration of the adsorbed dye molecules on TiO_2 surface. From the Benesi−Hilderband (BH) plot, the equilibrium constant of the adsorbed dye has been found to be 2.22×10^4 M^{-1}.We have also carried out steady-state absorption of C-343 on TiO_2 nanoparticle surface with increasing particle concentration. With increasing TiO_2 concentration, the optical absorption spectra of C-343 becomes broad and a little red shifted. The equilibrium constant of the adsorbed dye is determined from BH plot and found to be 1.45×10^4 M^{-1}.

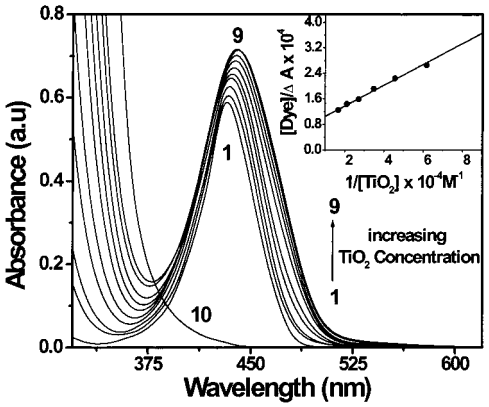

Figure 2. Absorption spectra of 7-diethyl amino coumarin 3-carboxylic acid (D-1421) dye in the presence of various TiO_2 concentration. Conditions: 12 μm D-1421 dye in 1 cm optical path length. TiO_2 concentrations are (1) 0.0, (2) 0.1, (3) 0.21, (4) 0.32, (5) 0.44, (6) 0.57, (7) 0.73, (8) 0.94, and (9) 1.19 gm/L. (10) Absorption spectrum of 10 gm/Lit TiO_2 nanoaprticle in water. pH of all the above solutions is 2.5. (Inset: Benesi-Hildebrand plot of the D-1421/TiO_2 complex monitoring at 500 nm).

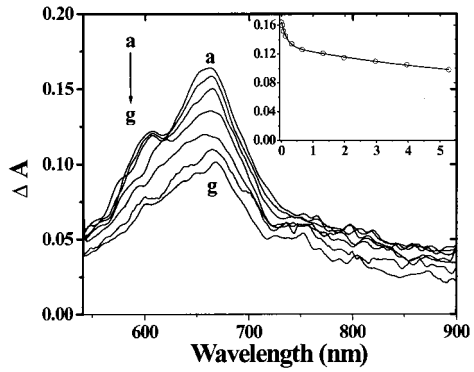

Figure 3. Transient absorption spectra of 7-diethyl amino coumarin 3-carboxylic acid (D-1421) (100 μM) sensitized TiO_2 colloid (20 gm/L) in water at (a) 35 ps, (b) 66 ps, (c) 132 ps, (d) 660 ps, (e) 1.32 ns, (f) 1.98 ns, and (g) 3.96 ns after 532 nm excitation. The spectrum at each time delay consists of a positive peak at 665 nm along with a shoulder at 610 nm and a broad positive absorption feature in the whole spectral region (750−900 nm). These features are assigned to the cation radical of D-1421 and injected electron in nanoparticle. [Inset: Kinetic decay trace of D-1421 cation radical at 665 nm].

It has been observed that D-1421 gives fluorescence in water, peaking at 470 nm with moderate quantum yield ($\phi = 0.022$). In the presence of the TiO_2 nanoparticle in water, the fluorescence of D-1421 gets quenched drastically. This has been attributed to electron injection from excited D-1421 to the conduction band of nanoparticle. However, a broad red-shifted low-quantum-yield fluorescence ($\phi \sim 0.0002$) peaking at 485 nm is observed in the present system. Emission behavior of the dye molecules has been discussed in detail in section f. Emission experiments for D-1421 on ZrO_2 nanoparticle are also carried out to see the fluorescence of D-1421 on a noninjecting surface and has been discussed in detail in section f.

(b) Assignment of Transient Absorption Spectra. Time-resolved experiments using picosecond flash photolysis have been carried out to study the electron-transfer processes in D-1421-sensitized TiO_2 nanoparticle system. Shown in Figure 3 is the picosecond transient absorption spectrum of the D-1421-sensitized TiO_2 colloid at different time delays following the 532 nm photoexcitation. The spectrum at each time delay

consists of a positive peak at 665 nm along with a hump at 610 nm and a broad positive feature in the whole spectral region (700−900 nm). The peak at 665 nm with a hump at 610 nm is assigned to the D-1421 cation radical. Assignment of this band has been made on the basis of a separate pulse radiolysis experiments where the D-1421 cation radical was generated selectively by the reaction of $N_3^{\bullet}$ radical (see next section). The broad feature in the 700−900 nm region is assigned to the electrons injected in to TiO_2 nanoparticles.[47−49] It has already been shown by many workers that conduction band electrons can be detected by visible[3−5,47−49] and infrared absorption.[24−30] To ensure that the observed transient absorption spectra are due to the photoexcitation of the D-1421-sensitized TiO_2 colloid, experiments with unsensitized TiO_2/water and D-1421/water are performed. No transient signals have been observed from these blanks following 532 nm excitation. It should be pointed out that the ground-state UV−vis spectrum of TiO_2 colloid shows no absorbance at 532 nm. Electron injection process has been explained in the equation below, where D-1421$^+$ is the excited state and cation radical of D-1421 dye and e_{cb}^- is the conduction band electron in TiO_2 nanoparticle. However, the cation radical absorbance band shows decay (Figure 3 Inset) and is due to the back reaction of conduction band electron and the parent D-1421 cation radical and is shown as

$$TiO_2 + \text{D-1421} \xrightarrow[\text{electron injection}]{h\nu} e^-_{cb}(TiO_2) + \text{D-1421}^+$$

$$e^-_{cb}(TiO_2) + \text{D}-1421^+ \xrightarrow{\text{recombination}} TiO_2 + \text{D-1421}$$

The decay of the observed signal due to the cation radical can be fitted with multiexponential function with time constants of 180 ps and >5 ns, Although up to 6 ns (our maximum time limit) only 60% of the cation signal decays, in longer time scale measurements (up to 1000 μs) the recombination process is also found to be a multiexponential process.[50] The back-electron-transfer dynamics in the case of the $Fe(CN)_6^{4-}$-sensitized TiO_2 nanoparticle studied by Ghosh et al.[27] was also found to be nonexponential. The origin of the nonexponential recombination was attributed to the spatial and energetic distribution of trap states for the injected electrons in the nanoparticles. So in these measurements it is also expected that the back-electron-transfer reactions for the D-1421-sensitized TiO_2 nanoparticles will be nonexponential.

(c) Detection of Cation Radical of D-1421 and C-343 Using Pulse Radiolysis Techniques. In the present investigation we are interested in comparing the electron injection efficiency of the D-1421 and C-343 dyes adsorbed on TiO_2 nanoparticle. Pico-second transient absorption studies are carried for both dyes sensitized TiO_2 nanoparticle and the transient absorption of the cation radicals has been monitored for the purpose (next section). To find out the transient absorption spectra of the cation radicals of the D-1421 and C-343 dyes and the molar extinction coefficients of those radicals at different wavelengths, pulse radiolysis experiments are carried out. In pulse radiolysis experiment one-electron oxidation reaction is studied in N_2O-saturated aqueous solution containing 10^{-4} mol dm^{-3} coumarin dyes and NaN_3 (5×10^{-2} mol dm^{-3}). The coumarin dyes are oxidized to cation radical by reacting with azide radical undergoing one-electron oxidation, i.e., loss of an electron. The reactions are given below:

$$H_2O \rightsquigarrow H^{\bullet}, OH^{\bullet}, e_{eq}^-, \text{etc.}$$

$$e_{aq}^- + N_2O \rightarrow N_2 + O^{\bullet -}$$

$$O^{\bullet -} + H_2O \rightarrow OH^{\bullet} + OH^-$$

$$N_3^- + OH^{\bullet} \text{ (or } O^{\bullet -}) \rightarrow N_3^{\bullet} + OH^- \text{ (or } O^{2-})$$

$$N_3^{\bullet} + \text{coumarin} \rightarrow N_3^- + \text{coumarin}^{\bullet +}$$

Now the corrected absorption spectra of the coumarin cation radicals are obtained in the following way. The difference absorption spectrum of the coumarin cation radical is corrected by applying a correction factor for the parent depletion. At a given wavelength λ, the molar absorption coefficient (ϵ_R) of the cation radical follows a simple relations as

$$\epsilon_R = \epsilon_G + \frac{\Delta A_{obs} G_{(SCN)_2^{\bullet -}} \epsilon_{(SCN)_2^{\bullet -}}}{A_{(SCN)_2^{\bullet -}} G_R}$$

where $A_{(SCN)_2^{\bullet -}}$ is the absorbance of $(SCN)_2^{\bullet -}$ at 500 nm observed in an air-saturated solution of KSCN (5×10^{-2} mol dm^{-3}) under the same experimental conditions. The values $G_{(SCN)_2^{\bullet -}} = 2.9$ and $\epsilon_{(SCN)_2^{\bullet -}} = 7100$ dm^3 mol^{-1} cm^{-1} are used for the calculation.[45] G_R for water is used to be 6.0.[51] ϵ_G is the molar absorption coefficients of the parent. The corrected absorption spectra of the D-1421 and C-343 cation radical are given in parts a and b of Figure 4, respectively. The molar absorption coefficients of D-1421 cation radical at the peak wavelength i.e., 665 nm is calculated to be 3.2×10^3 dm^3 mol^{-1} cm^{-1} and for C-343 cation radial at the peak wavelength, i.e., 635 nm is calculated to be 2.8×10^3 dm^3 mol^{-1} cm^{-1}.

(d) Quantum Yield of Electron Injection of D-1421 and C-343. We have performed picosecond laser flash photolysis study of D-1421- and C-343-sensitized TiO_2 nanoparticle to determine the electron injection efficiency of the above systems. Figure 5a shows the spectrum of D-1421-sensitized TiO_2 nanoparticle excited by 532 nm at the end of the pulse (0 ps). To compare the injection efficiency, experiments have also been carried out in C-343-sensitized TiO_2 nanoparticle in similar condition and are shown in Figure 5b. Same laser intensity was kept for both the cases. The laser intensity has been measured by monitoring the excited singlet state of C_{60} at 885 nm (6.3×10^3 dm^3 mol^{-1} cm^{-1}).[52] The extinction coefficient of the D-1421 cation radical at 665 nm is determined to be 3.2×10^3 dm^3 mol^{-1} cm^{-1} and for the C-343 cation radical at 635 nm is 2.8×10^3 dm^3 mol^{-1} cm^{-1} (previous section). Now, from the transient absorption of D-1421 and C-343-sensitized nanoparticle systems, the quantum yields for the electron injection (ϕ_{cation}) are found to be 0.90 and 0.60, respectively. In the present investigation we have already discussed that excitation of free dye does not give any cation radical at the laser intensity used. The point to be noted that the free dye solutions of D-1421 and C-343 in water do not absorb 532 nm laser light at the concentration used in the above experiments. So the ϕ_{cation} can be attributed to the $\phi_{injection}$.

(e) Solvatochromic Behavior of D-1421 and C-343. Although the basic structures of the two dyes (D-1421 and C-343) are very similar (Figure 1), the couplings with the TiO_2 nanoparticle are same (both the dyes are having same anchoring group with the nanoparticle), still we have observed 50% more electron injection in the case of the D-1421-sensitized TiO_2 nanoparticle. To find out the mechanism of efficient electron injection, we have carried out solvatochromic measurements for the coumarin dyes (D-1421 and C-343). We have carried out steady-state absorption and emission measurements and time-resolved emission measurements for both the dyes in different solvents and solvent mixtures changing their polarity. The

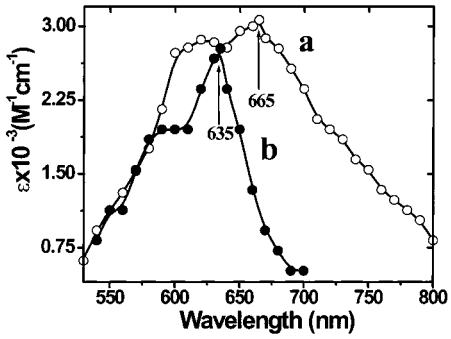

Figure 4. Transient absorption spectra of the cation radicals of (a) D-1421 and (b) C-343 as obtained from pulse-radiolysis experiments. The experiments were carried out dissolving the dyes (10^{-4} M) and N_3^- (50×10^{-3} mM) in water and saturating with N_2O.

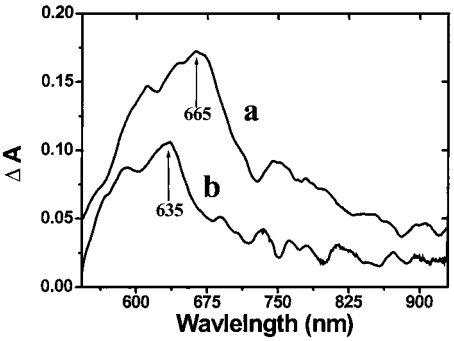

Figure 5. Transient absorption spectra of (a) D-1421-sensitized TiO_2 nanoparticle and (b) C-343-sensitized TiO_2 nanoparticle after exciting at 532 nm (fwhm =35 ps) at the end of the laser pulse. The laser intensity in both the cases was kept same.

absorption spectra of both the coumarin dyes undergo only small red shift with increasing solvent polarity. The fluorescence maxima (λ_{fl}) and half bandwidth ($\Delta\nu_{1/2}$) of the coumarins are independent of excitation wavelength.

The Stokes' shifts, ($\Delta\nu_{st}$), for both the coumarins are calculated from the maxima of the absorption and fluorescence spectra. Shown in Figure 6A is a plot of the Stokes' shift vs the solvent parameter Δf expressed in the following equation[53]

$$\Delta f = \frac{\epsilon - 1}{2\epsilon + 1} - \frac{n^2 - 1}{2n^2 + 1}$$

that describes the solvent polarity and polarizability and is calculated from the dielectric constant ϵ and the refractive index n. The slopes in Figure 6A mainly determined by the solvent dependence of the fluorescence maxima. From Figure 6A it is evident that both the dyes are charge transfer in nature in polar solvents. These results indicate that, the first excited state of both the coumarin dyes exist as intramolecular charge transfer (ICT) state. Many workers have made similar observations for other coumarin dyes.[54] The linear dependency of $\Delta\nu$ vs Δf in Figure 6A shows that the emission comes from single state for both the dyes and is from ICT state.

To get into the detail of the problem, we have measured the fluorescence quantum yield (ϕ_f) and fluorescence lifetime (τ_f) for both the dyes (D-1421 and C-343) in different solvents and solvent mixtures. Shown in Figure 6B is the plot of ϕ_f vs the solvent parameter Δf. It has been observed in the plot that, in the case of C-343, the fluorescence quantum yield (ϕ_f) decreases monotonically as we increase the solvent polarity. But it is very interesting to see the results obtained for D-1421 with changing the solvent polarity. It is seen in Figure 6B, that for D-1421,

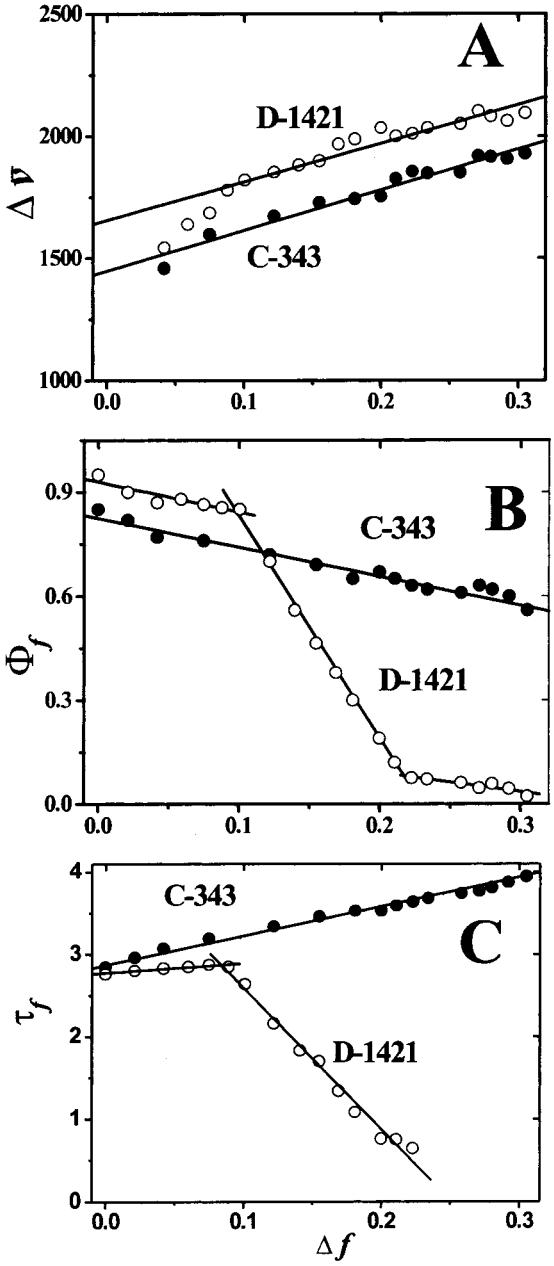

Figure 6. Plot of the (A) Stokes shifts ($\Delta\nu$), (B) emission quantum yields (Φ_f), and (C) emission lifetime (τ_f) for D-1421 and C-343 in different solvents and solvent mixtures against Δf value of the solvents ($\Delta f = (\epsilon - 1/2\epsilon + 1) - (n^2 - 1/2n^2 + 1)$ where ϵ is the dielectric constant and n^2 is the refractive index of the solvent).

initially as we increase the polarity of the solvent, the fluorescence quantum yield (ϕ_f) decrease gradually. And then if we increase the solvent polarity more, ϕ_f decreases drastically with different slope. At high polar solvent the fluorescence quantum yield (ϕ_f) is very low. These results indicate that after certain polarity there is one more fast de-excitation pathway for the excited singlet state. We have also carried out the time-resolved measurements to determine the fluorescence lifetime (τ_f) for both the dyes and are plotted in Figure 6C. It is seen in the plot that for C-343 the fluorescence lifetime (τ_f) increases monotonically as we increase the polarity of the solvent. This is because in high polar solvent the excited state is ICT state, which has higher radiative lifetime. But in the case of D-1421, as we increase the polarity of the solvent, initially the τ_f increases, and then it decreases drastically with different slope (Figure 6C). At high polar solvent the emission of D-1421 decays

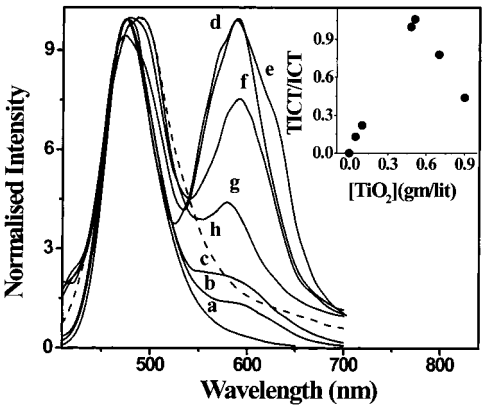

Figure 7. Normalized emission spectra of D-1421 dye (12 μM) molecule in water with increasing concentration of TiO_2 nanoparticle. TiO_2 concentrations are (a) 0.00 (ϕ_{em}= 0.022), (b) 0.05, (c) 0.10, (d) 0.51, (e) 0.48, (f) 0.70, (g) 0.90, and (h) 15 gm/L (ϕ_{em}= 0.0002). The pH of all the solutions is 2.5. With increasing TiO_2 concentration emission quantum yield decreases drastically.

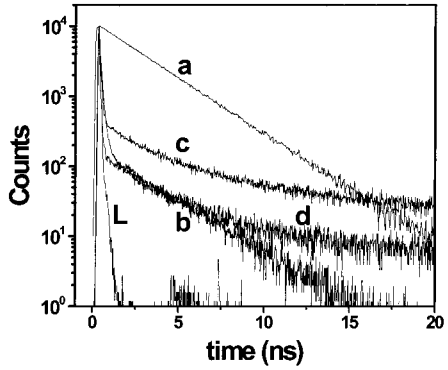

Figure 8. Single-photon-counting studies of D-1421 dye in different media, (a) in methyl cyclohexane (λ_{em} = 430 nm), (b) in water (λ_{em} = 470 nm), (c) in TiO_2 colloid (0.33 gm/L) (λ_{em} = 590 nm), and (d) in TiO_2 colloid (5.0 gm/L) (λ_{em} = 590 nm) after 445 nm excitation.

nonexponentially. This sudden decrease in fluorescence quantum yield (ϕ_f) and fluorescence lifetime (τ_f) with increasing polarity can be explained by twisted intramolecular charge transfer state (TICT) mechanism.

As we have discussed, at high polarity solvent the decay of D-1421 emission decay is nonexponential. Figure 8 shows the emission decay traces of D-1421 in methyl cyclohexane (τ_{em} = 2.75 ns) (Figure 8a) and in water (Figure 8b) (next section). The emission decay time in water is very short (τ_{av} < 20 ps). It has already been observed by Rettig et al.[37,55] that the emission from DMABEE (dimethyl amino benzoic acid ethyl ester) decays nonexponentially with very short lifetime in high polar solvent. They have explained that on excitation the molecule goes to the LE (locally excited) or ICT state and then very fast relaxes to the TICT state. Nonradiative decay rates for the above molecule have been found to be very high. The transition from LE/ICT state to TICT has been attributed to barrierless.[55] In the present study also we can attribute that for D-1421 molecule transition from ICT to TICT as barrier less. As a result of which we can see nonexponential decay in high polar solvent. It has also been observed that the nonradiative decay channels from ICT state for D-1421 molecule are very fast in high polarity solvent.

(f) Detection of TICT Emission Band of D-1421 on TiO_2 Nanoparticle. It has been demonstrated by Nag et al.[56] that the TICT emission band of *p*-(*N*,*N*-dimethylamino) benzonitrile (DMABN) can be enhanced on complexation with cyclo dextrin (CD) molecule. It has also been observed by Kim et al. the enhancement of TICT emission of *p*-*N*,*N*-dimethylaminobenzoic acid (DMABA) in the zeolite moiety[57] and on the SiO_2 nanoparticle[58] surface in acetonitile solution. They have attributed it to the hydrogen bonding effect of the dye molecule with the OH^- group of the SiO_2 moiety of nanoparticle and zeolite surface. They have observed that enhancement of TICT emission band occurs up to certain concentration of nanoparticle in the dye−nanoparticle system. At a high concentration of the SiO_2 nanoparticle, again the intensity of the emission band decreases. To find out the TICT emission band of D-1421 molecule, we have carried out steady-state emission experiments with changing TiO_2 nanopaticle concentration in water solution. It has already been discussed that in water and other high polar solvent (e.g., acetonitrile) TICT emission band could not be detected for the D-1421 molecule. The D-1421 molecule gives emission band peaking at 475 nm in water with quantum yield ϕ = 0.022 (Figure 7a). As we increase the TiO_2 nanoparticle concentration, the intensity of the emission band at 475 nm decreases drastically. This is due to electron injection in the conduction band of the nanoparticle. On normalization of the emission bands of the dye molecule at different TiO_2 nanoparticle concentration, we have observed that the original band gets little red-shifted and a new band appears at 585 nm (Figure 7). Initially, with increasing TiO_2 concentration, the emission intensity of the band at 585 nm increases. The intensity of the band (585 nm) at a higher TiO_2 nanoparticle concentration decreases. We are attributing the band at 585 nm for the D-1421 molecule to the TICT emission. Figure 7 inset shows the ratio of TICT and ICT emission (I_{TICT}/I_{ICT}) with increasing TiO_2 concentration. On adsorption dye molecule on nanoparticle surface, emission from TICT state facilitates due to binding with the nanoparticle. Enhancement of TICT emission of DMABA molecule was also observed on SiO_2 nanoparticle surface.[58] It was also observed that at high SiO_2 concentration again TICT emission yield decreases. In the present investigation also we have observed similar enhancement of TICT emission of the D-1421 molecule on the TiO_2 nanoparticle surface. In neat water, the TICT state of the D-1421 molecule is not emissive, but in the presence of little TiO_2 concentration the D-1421 molecules form hydrogen bonds with nanoparticles and they enhance the emission property and give emission.

In Figure 7 we have observed that with increasing TiO_2 concentration the relative intensity of the TICT band initially increases and then it decreases. In neat water, the TICT state of D-1421 is not emissive. In presence of little TiO_2 concentration, the D-1421 molecules form hydrogen bonds with nanoparticles and they enhance the emission property of TICT and give second emission band. But total emission quantum yield always decreases as we increase the TiO_2 concentration. Initial increment of the TICT band intensity is due to extra formation of hydrogen bonds. This can be explained in the following way. At initial stage (Figure 7) the TiO_2 in the solution is lower, so the relative dye concentration is higher, at this stage some dye molecules will be on the surface and some of them will be in the bulk. The dye molecules, which are strongly adsorbed on the surface, will inject electrons, and the dye molecules which are weakly hydrogen bonded will be yielding the TICT state but many of the dye molecules will be in the bulk and will have higher quantum yields of the ICT state. So the TICT emission will be masked. As we increase the TiO_2 concentration, more and more dye molecules will come on to the surface and relative ICT emission will decrease and TICT emission will increase. At 0.5 gm/L TiO_2 concentration, all the dye molecules

TABLE 1: Emission Life Times of D-1421 in Different Media Exciting at 444 nm (fwhm = 4ps) Laser light

sample	$\lambda_{em} = 470$ nm	$\lambda_{em} = 590$ nm
D-1421/water	$\tau_1 = 0.023$ (77.4%)	$\tau_1 = 0.021$ (87.0%)
	$\tau_2 = 0.129$ (21.7%)	$\tau_2 = 0.128$ (12.6%)
	$\tau_3 = 2.813$ (0.9%)	$\tau_3 = 2.681$ (0.4%)
D-1421/TiO_2 colloid (0.07 g/L)[a]	$\tau_1 = 0.027$ (96.7%)	$\tau_1 = 0.026$ (97.3%)
	$\tau_2 = 0.118$ (2.2%)	$\tau_2 = 0.093$ (2.0%)
	$\tau_3 = 2.851$ (1.1%)	$\tau_3 = 2.833$ (0.64%)
		$\tau_4 = 17.86$ (0.06%)
D-1421/TiO_2 colloid (0.16 g/L)[a]	$\tau_1 = 0.028$ (96.8%)	$\tau_1 = 0.025$ (97.2%)
	$\tau_2 = 0.110$ (1.2%)	$\tau_2 = 0.073$ (2.1%)
	$\tau_3 = 2.851$ (1.9%)	$\tau_3 = 2.636$ (0.6%)
		$\tau_4 = 20.514$ (0.1%)
D-1421/TiO_2 colloid (0.33 g/L)[a]	$\tau_1 = 0.026$ (97.9%)	$\tau_1 = 0.021$ (96.0%)
	$\tau_2 = 0.065$ (0.4%)	$\tau_2 = 0.081$ (3.0%)
	$\tau_3 = 2.73$ (1.8%)	$\tau_3 = 2.396$ (0.8%)
		$\tau_4 = 21.662$ (0.2%)
D-1421/ TiO_2 colloid (5.0 g/L)[a]	$\tau_1 = 0.014$ (98.5%)	$\tau_1 = 0.009$ (99.8%)
	$\tau_2 = 0.053$ (0.4%)	$\tau_2 = 0.235$ (0.02%)
	$\tau_3 = 2.74$ (1.1%)	$\tau_3 = 2.276$ (0.16%)
		$\tau_4 = 17.906$ (0.02%)

[a] TiO_2 concentration in water.

adsorbed on the surface and the strong complexes inject electron but relatively weaker complexes, i.e., H-bonded complexes will give the TICT state. Now again when we increase TiO_2 concentration most of the dye molecules will go for stronger complexes and will inject electrons, and the emission intensities of the TICT states will decrease. The point to be noted that the strong complexes will also give TICT states and that they also inject electrons.

We have also compared the photophysical properties of D-1421 on a noninjecting surface ZrO_2 nanoparticle. We have also carried out steady-state measurements with changing ZrO_2 concentration. At 0.5 gm/L of ZrO_2, we have observed a small TICT emission band at 590 nm. As the ZrO_2 is further increased, the TICT band disappears as in the case of TiO_2. This can be explained in the following way. At smaller concentration of nanoparticle, the number of dye molecules on the nanoparticle will be more and hence the dyes can form weak hydrogen bonding with the nanoparticle surface and can give TICT emission. As the nanoparticle concentration further increased, the number of dye molecules per particle decreases and weak hydrogen bonded dye−nanoparticle complexes decreases and hence TICT emission decreases.

To support the above observation we have carried out time-resolved emission studies on the D-1421-sensitized TiO_2 nanoparticles with changing particle concentrations, and monitoring at two different emission wavelengths, 470 and 590 nm, respectively (Table 1). All the emission traces decay very fast and nonexponentially. We have forcefully fitted the data with a multiexponential function. Figure 8b shows the decay trace of D-1421 in water at 470 nm and fitted with multiexponential function with three time constants (Table 1). Figure 8, parts c and d, shows the decay traces of D-1421-sensitized TiO_2 nanoparticle in 0.33 gm/L and in 5 gm/L, monitored at 590 nm. Emission at 470 nm has been fitted with three exponentials; where as emission at 590 nm has been fitted with four exponentials (Table 1). First two components in all the traces decay very fast and they contributes maximum (~99%). These two components can be attributed to the fast nonexponential decay. The third long component in all the decay trace has been attributed to the singlet state lifetime (~2.5−2.8 ns) of D-1421

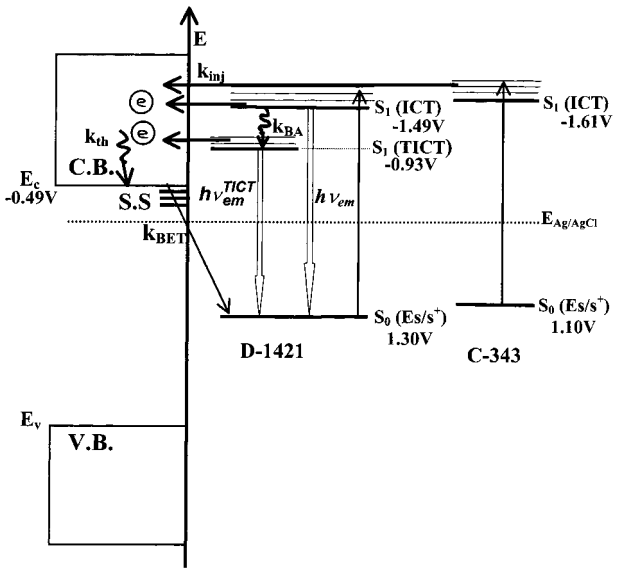

Figure 9. Mechanistic scheme for electron transfer from the electronically excited dye to TiO_2 nanoparticle. Here S^*/S^+ is the excited sensitized dye/cation radical couple, E_c the conduction band edge, E_v the valence band, SS the surface states, ICT is the intramolecular charge transfer state, and TICT is the twisted intramolecular charge transfer state. k_{BET} is the back-electron-transfer rate, k_{BA} is the relaxation rate from ICT state to TICT state. $h\nu_{em}^{ICT}$ indicates emission from ICT state and $h\nu_{em}^{TICT}$ indicates emission from TICT state.

in water and on nanoparticle surface. The fourth long component for the traces 8c and 8d has been attributed to the emission lifetime (~20 ns) of the TICT state of D-1421. We have also observed that with changing TiO_2 concentration, the relative contribution of TICT state changes as we observed in Figure 7.

(g) Mechanism of Electron Injection from TICT State. In normal dye-sensitization nanoparticle system, electron injection takes place via excited state of the dye[59] (Figure 9). On excitation by laser pulse the dye molecule goes to the excited state. The excited molecular state of the dye molecule overlaps with manifold acceptor states of the nanoparticle conduction band.[59] It means that all the vibrational and rotational states of the excited electronic state of the dye molecule overlap with the conduction band. Electron transfer from the excited dye molecule is possible from all vibrational states. So electron injection and vibrational relaxation take place together. This has been reported by Asbury et al.:[33] electron injection occurred during or prior to electronic and vibrational relaxation of the sensitizer molecules in the excited state; in the process, 100% electron injection is not possible. A good portion of the excited dye molecules will relax to ground vibrational state of the first excited electronic state; from there, nonradiative and radiative (emission) processes are possible. In most of the dye sensitization process, other than electron injection, deexcitation processes take place via nonradiative and radiative transfer. In the case of C-343-sensitized nanoparticle the above processes takes place.

The energetics of the ground and excited oxidation potentials of the dye molecules and the conduction band of the semiconductor has shown in Figure 9. The GS oxidation potential for the dyes was measured by cyclic voltametry against Ag/AgCl electrode. The dye oxidations are reversible. The excited oxidation potential of the dyes were measured by adding the E_{00} and GS oxidation potential. E_{00} has been measured from the crossing point of the excitation and emission spectra of the dye molecules. The energetics of the TICT state of D-1421 molecule has been determined from the shift in energy from the ICT state to the TICT state in Figure 7. The conduction

band potential of TiO_2 nanoparticle has been calculated from the following equation[60]

$$E_{CB}(TiO_2) = -(0.12 \pm 0.02) - 0.059(pH)\ V\ (vs\ NHE)$$

E_{CB} at pH 2.5 has been calculated to be −0.267 (vs NHE) and −0.49 (vs Ag/AgCl) (Figure 9).

It has been observed from Figure 9, in the D-1421-sensitized TiO_2 nanoparticle system, upon excitation by laser pulse the dye molecule goes to the excited state (ICT) and then it relaxes very fast to the TICT state. Electron transfer can take place more easily and efficiently from TICT state compare to any other state. At the same time other deactivation channel like radiative (emission) transitions to the ground state are forbidden. So the main deactivation channel is the electron transfer to the conduction band. As a result, we can see efficient electron injection from the D-1421 molecule to TiO_2 nanoparticle compared to that of C-343 to the TiO_2 nanoparticle. The higher measured injection yield measured in the case of the D-1421-sensitized TiO_2 nanoparticle other than the TICT state injected into the nanoparticle indicated that there may be a lower degree of geminate recombination because the LUMO of $D\text{-}1421^+$ is localized in the diethyl amino group. But the recombination effect will be more prominent in the longer time scale. As here we have measured the injection yield at the end of the laser pulse, so higher injection yield will be mostly responsible for the electron injection from the TICT state.

Conclusions

Picosecond transient absorption and time-resolved emission spectroscopy have been used to study the effect of structure in photoinduced electron-transfer dynamics in coumarin dye (D-1421 and C-343)-sensitized TiO_2 nanoparticle in aqueous solution. The molecular structures of the studied dyes (D-1421 and C-343) are very similar with same anchoring group which bind to the TiO_2 nanoparticle, except D-1421 has the free diethyl amino group and the nitrogen atom is in the ring for C-343. Electron injection has been confirmed by direct detection of conduction band electron in 700−900 nm region and cation radical in the visible region as we excite the dye (both D-1421 and C-343)-sensitized TiO_2 nanoparticle by 532 nm picosecond laser. The assignment of cation radical of the coumarin dyes was confirmed by pulse-radiolysis technique. Electron injection efficiency was found to be much higher for the D-1421-sensitized TiO_2 nanoparticle ($\phi_{inj} = 0.90$) compared to the C-343-sensitized TiO_2 nanoparticle ($\phi_{inj} = 0.60$). Steady-state and time-resolved fluorescence measurements show that, in the excited state, the D-1421 dye undergoes twisted intramolecular charge transfer (TICT) in highly polar solvents, whereas C-343 does not. On excitation, the C-343 molecule goes to the ICT (intramolecular charge transfer) state. On the other hand, on excitation the D-1421 dye molecule goes to the ICT state and then very fast it relaxes to the TICT state. High charge separation process takes place within the molecule in high polarity solvents in the TICT state compared to that of the ICT state. Electron injection for the D-1421 dye can take place both from the ICT state and the TICT state. But TICT is a higher charge-separated state: it can inject electron more efficiently to the TiO_2 nanoparticle compare to ICT state. On the other hand, the TICT state has a higher lifetime than the ICT state, because transitions (radiative and nonradiative) from the TICT state to the GS (ground state) are forbidden, allowing more time to inject the electron. Quantum yield for electron injection for D-1421 dye is found to be 0.90 compared to 0.60 for C-343. The TICT state of D-1421 is nonemissive in all solvents (polar and nonpolar). But emission from the TICT state has been observed from the D-1421 molecule on the TiO_2 nanoparticle surface. Research in this direction will help us to find out the conditions for getting more efficiency in dye-sensitized solar cells. Our ongoing experiments are carried out in different dye-sensitized TiO_2 nanoparticle systems, particularly the dyes which yield the TICT state upon excitation in polar solvent, to get more insights of electron injection from the TICT state.

Acknowledgment. We thank Mr. A. S. R. Koti of the Tata Institute of Fundamental Research, Mumbai, India, for his assistance in the time-resolved fluorescence measurements, and Dr. P. A. Hassan and Mrs. Shilpa Tawde of NM & SC Division, BARC, Mumbai, for their assistance in cyclic voltametry measurements. We are also thankful to Dr. A. V. Sapre, Dr. T. Mukherjee and Dr. J. P. Mittal for their encouragement.

References and Notes

(1) Oregan, B.; Gratzel, M. *Nature* **1991**, *353*, 737.
(2) Hagfeldt, A.; Gratzel, M. *Chem. Rev.* **1995**, *95*, 49.
(3) Ghosh, H. N. *J. Phys. Chem. B* **1999**, *103*, 10382.
(4) Ramakrishna, G.; Ghosh, H. N. *J. Phys. Chem. B* **2001**, *105*, 7000.
(5) Ramakrishna, G.; Ghosh, H. N.; Singh, A. K.; Palit, D. K.; Mittal, J. P. *J. Phys. Chem. B* **2001**, *105*, 12786.
(6) Martini, I.; Hodak, J. H.; Hartland, G. V.; Kamat, P. V. *J. Chem. Phys.* **1997**, *107*, 8064.
(7) Martini, I.; Hartland, G. V.; Kamat, P. V. *J. Phys. Chem. B* **1997**, *101*, 4826.
(8) Martini, I.; Hodak, J. H.; Hartland, G. V. *J. Phys. Chem. B* **1998**, *102*, 607.
(9) Martini, I.; Hodak, J. H.; Hartland, G. V. *J. Phys. Chem. B* **1998**, *102*, 9508.
(10) Hilgendroff, M.; Sundstrom, V. *Chem. Phys. Lett.* **1998**, *287*, 709.
(11) Hilgendroff, M.; Sundstrom, V. *J. Phys. Chem. B.* **1998**, *102*, 10505.
(12) Benko, G.; Hilgendroff, M.; Yartsev, A. P.; Sundstrom, V. *J. Phys. Chem. B* **2001**, *105*, 967.
(13) Moser, J.; Graetzel, M. *J. Am. Chem. Soc.* **1984**, *106*, 6557.
(14) Kamat, P. V.; Fox, M. A. *Chem. Phys. Lett.* **1983**, *102*, 379.
(15) Moser, J. E.; Gratzel, M.; Sharma, D. K.; Serpone, N. *Helv. Chim. Acta* **1985**, *68*, 1686.
(16) Eichberger, R.; Willig, F. *Chem. Phys.* **1990**, *141*, 159.
(17) Lanzafame, J. M.; Miller, R. D. J.; Muenter, A. A.; Parkinson, B. A. *J. Phys. Chem.* **1992**, *96*, 2820.
(18) Heimer, T. A.; Heilweil, E. J. *J. Phys. Chem. B* **1997**, *101*, 10990.
(19) Lu, H.; Prieskorn, J. N.; Hupp, J. T. *J. Am. Chem. Soc.* **1993**, *115*, 4927.
(20) Dang, X.; Hupp, J. T. *J. Am. Chem. Soc.* **1999**, *121*, 8399.
(21) Kuciauskas, D.; Freund, M. S.; Gray, H. B.; Winkler, J. R.; Lewis, N. S. *J. Phys. Chem. B* **2001**, *105*, 392.
(22) Argazzi, R.; Bignozzi, C. A.; Heimer, T. A.; Castellano, F. N.; Meyer, G. J. *J. Am. Chem. Soc.* **1995**, *117*, 11816.
(23) Weng, Y.; Wang, Y.; Asbury, J. B.; Ghosh, H. N.; Lian, T. *J. Phys. Chem. B* **2000**, *104*, 93.
(24) Ghosh, H. N.; Asbury, J. B.; Lian, T. *J. Phys. Chem. B* **1998**, *102*, 6482.
(25) Ghosh, H. N.; Asbury, J. B.; Lian, T. *Proc. Ind. Nat. Sci. Acad.* (PINSA) *A* **2000**, *66*, 177.
(26) Ghosh, H. N.; Asbury, J. B.; Lian, T. To be published.
(27) Ghosh, H. N.; Asbury, J. B.; Weng, Y.; Lian, T. *J. Phys. Chem. B* **1998**, *102*, 10208.
(28) Ellingson, R. J.; Asbury, J. B.; Ferrere, S.; Ghosh, H. N.; Lian, T.; Nozik, A. *J. Phys. Chem. B* **1998**, *102*, 6455.
(29) Asbury, J. B.; Ellingson, R. J.; Ghosh, H. N.; Ferrere, S.; Nozik, A.; Lian, T. *J. Phys. Chem.* **1999**, *103*, 3110.
(30) Asbury, J. B.; Hao, E.; Wang, Y. Q.; Ghosh, H. N.; Lian, T. *J. Phys. Chem. B* **2001**, *105*, 4545 (Feature Article).
(31) Haque, S. A.; Tachibana, Y.; Klug, D. R.; Durrant, J. R. *J. Phys. Chem. B* **1998**, *102*, 1745.
(32) Asbury, J. B.; Hao, E.; Wang, Y.; Lian, T. *J. Phys. Chem.* **2000**, *104*, 11957.
(33) Asbury, J. B.; Wang, Y. Q.; Hao, E.; Ghosh, H. N.; Lian, T. *Res. Chem. Intermed.* **2001**, *27*, 393.
(34) Bonhote, P.; Moser, J. E.; Humphry-Baker, R.; Vlachopoulos, N.; Zakeeruddin, S. M.; Walder, L.; Gratzel, M. *J. Am. Chem. Soc.* **1999**, *121*, 1324.

(35) Vogel, M.; Rettig, W. *Ber. Bunsen-Ges. Phys. Chem.* **1985**, *89*, 962.
(36) Rettig, W. *Angew. Chem.* **1986**, *25*, 971.
(37) Lippert, E.; Rettig, W.; Bonacic-Koutecky, V.; Heisel, F.; Miehe, J. A. *Adv. Chem. Phys* **1987**, *68*, 1.
(38) Rettig, W. *Topics in Current Chemistry. 169. Electron-Transfer I*; Mattay, J., Ed.; Springer-Verlag: Berlin, 1994; p 254.
(39) Lueck, H.; Windsor, M. W.; Rettig, W. *J. Phys. Chem.* **1990**, *94*, 4550.
(40) Bahnemann, D.; Henglein, A.; Lilie, J.; Spanhel, L. *J. Phys. Chem.* **1984**, *88*, 709.
(41) Ghosh, H. N.; Adhikari, S. *Langmuir* **2001**, *17*, 4129.
(42) Ghosh, H. N.; Pal, H.; Sapre, A. V.; Mittal, J. P. *J. Am. Chem. Soc.* **1993**, *115*, 11722.
(43) O'Connor, D. V.; Phillips, D. *Time Correlated Single Photon Counting*; Academic Press: New York, 1984.
(44) Mukherjee, T. In *Atomic, Molecular and Cluster Physics*, Ahmad, S. A., Ed.; Narosa: New Delhi, 1997; p 299.
(45) Adams, G. E.; Boag, J. W.; Current, J.; Michael, B. D. In *Pulse Radiolysis*; Ebert, M., Keene, J. P., Swallow, A. J., Baxendale, J. H., Eds.; Academic Press: London, 1965; p 117.
(46) Yarwood, J. *Spectroscopy and Structure of Molecular Complexes*; Plenum Press: New York, 1970.
(47) Zhang, J. Z. *Acc. Chem. Res.* **1997**, *30*, 423.
(48) Colombo, D. P., Jr.; Bowman, R. M. *J. Phys. Chem.* **1996**, *100*, 18445.
(49) Skimmer, D. E.; Colombo, D. P., Jr.; Cavaleri, J. J.; Bowman, R. M. *J. Phys. Chem.* **1995**, *99*, 7853.
(50) Ramakrishna, G.; Ghosh, H. N. Unpublished work, 2001.
(51) Schuler, R. H.; Patterson, L. K.; Janata, E. *J. Phys. Chem.* **1980**, *84*, 2088.
(52) Palit, D. K.; Sapre, A. V.; Mittal, J. P. *Ind. J. Chem.* **1992**, *31A*, *B*, F 46.
(53) Mataga, N.; Kaifu, Y.; Koizumi, M. *Bull. Chem. Soc. Jpn.* **1955**, *28*, 690.
(54) Jones, G., II; Jackson, W. R.; Choi, C.; Bergmark, W. R. *J. Phys. Chem.* **1985**, *89*, 294.
(55) Rettig, W.; Wermuth, G. *J. Photochemistry* **1985**, *28*, 351.
(56) Nag, A.; Bhattacharya, K. *Chem. Phys. Lett.* **1988**, *151*, 474.
(57) Kim, Y.; Lee, B. I.; Yoon, M.; *Chem. Phys. Lett.* **1998**, *286*, 466.
(58) Kim, Y.; Cheon, H. W.; Yoon, M.; Song, N. W.; Kim, D. *Chem. Phys. Lett*. **1997**, *264*, 673.
(59) Miller, R. D. J.; McLendon, G. L.; Nozik, A. J.; Schmickler, W.; Willig, F. *Surface Electron-transfer Processes*; VCH publishers, Inc.: New York, 1995.
(60) Duonghong, D.; Ramsden, J.; Gratzel, M. *J. Am. Chem. Soc.* **1982**, *104*, 2977.